Inorganic Chemistry

Article

pubs.acs.org/IC

Temperature-Triggered Reversible Dielectric and Nonlinear Optical Switch Based on the One-Dimensional Organic–Inorganic Hybrid Phase Transition Compound $[C_6H_{11}NH_3]_2CdCl_4$

Wei-Qiang Liao,[†] Heng-Yun Ye,[†] Da-Wei Fu,[†] Peng-Fei Li,[†] Li-Zhuang Chen,[‡] and Yi Zhang*[,†]

[†]Ordered Matter Science Research Center, Southeast University, Nanjing 211189, People's Republic of China

[‡]School of Biology and Chemical Engineering, Jiangsu University of Science and Technology, Zhenjiang 212003, People's Republic of China

Supporting Information

ABSTRACT: The one-dimensional organic–inorganic hybrid compound bis(cyclohexylammonium) tetrachlorocadmate(II) (**1**), in which the adjacent infinite $[CdCl_4]_n^-$ chains are connected to each other though Cd···Cl weak interactions to form perovskite-type layers of corner-sharing $CdCl_6$ octahedra separated by cyclohexylammonium cation bilayers, was synthesized. It undergoes two successive structural phase transitions, at 215 and 367 K, which were confirmed by systematic characterizations including differential scanning calorimetry (DSC) measurements, variable-temperature structural analyses, and dielectric and second harmonic generation (SHG) measurements. A precise structural analysis discloses that the phase transition at 215 K is induced by the disorder–order transition of cyclohexylammonium cations, while the phase transition at 367 K derives from changes in the relative location of Cd atoms. Emphatically, both the dielectric constant and SHG intensity of **1** show a striking change between low and high states at around 367 K, which reveals that **1** might be considered as a potential dielectric and nonlinear optical (NLO) switch with high-temperature response characterization, excellent reversibility, and obvious change of states.

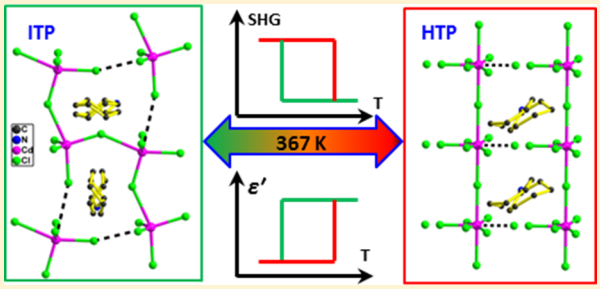

INTRODUCTION

Switchable materials, whose physical properties (optical, electrical, magnetic, and/or mechanical properties) can be reversibly modified between two or more relatively stable states by external stimuli such as light, temperature, and electric field, have attracted great attention for their wide application in the fields of photonic devices, optoelectronic technology, digital processing, sensors, etc.[1−5] Various approaches have been developed to design such materials, and a large number of materials possessing single-switchable electrical,[6−11] optical,[12−16] or magnetic[17,18] properties have been studied. However, there still exist two significant challenges: one is how to control the switching response characteristics by structural modulation and external stimuli and the other is how to obtain compounds with multiple switchable physical properties. One of the most feasible strategies is to construct temperature-triggered solid-to-solid structural phase transition materials, due to the fact that the physical properties often present abrupt changes near the phase transition point.[19−28] It is remarkable that the organic–inorganic hybrids offer an important opportunity to combine with the phase transition properties and multiple switching response characteristics. On the one hand, the organic–inorganic hybrids have been proven to be excellent candidates to prepare phase transition materials.[29−36] On the other hand, they provide the possibility of integrating desirable organic and inorganic characteristics within a single-crystalline molecular-scale composite, being able to achieve multifunctional characteristics.[37−47]

Encouraged by this strategy, we synthesized the novel one-dimensional organic–inorganic hybrid compound $[C_6H_{11}NH_3]_2CdCl_4$ (**1**), in which the neighboring infinite $[CdCl_4]_n^-$ chains are connected to each other by Cd···Cl weak interactions, forming perovskite-type layers of corner-sharing $CdCl_6$ octahedra separated by cyclohexylammonium cation bilayers. Systematic structure and property characterizations indicate that this compound undergoes two phase transitions at 215 and 367 K, respectively. In particular, **1** shows switchable dielectric and NLO behaviors in the vicinity of the higher phase transition temperature.

EXPERIMENTAL SECTION

Synthesis. Evaporation of an aqueous solution (100 mL) of cyclohexylamine hydrochloride (6.78 g, 0.05 mol) and cadmium chloride (5.7 g, 0.025 mol) at room temperature after several weeks results in the formation of **1** as large colorless platelike crystals (Figure S1, Supporting Information). In the IR spectra of **1** (Figure S2, Supporting Information), the band at 3117 cm^{-1} was assigned to the N–H stretching vibrations of the $-NH_3^+$ group. The $-NH_3^+$

Received: July 21, 2014
Published: October 3, 2014

   dx.doi.org/10.1021/ic501749c | *Inorg. Chem.* 2014, 53, 11146−11151

deformation vibrations were observed at 1597 and 1491 cm^{-1}. The experimental powder X-ray diffraction (PXRD) patterns match the simulated patterns very well in terms of the crystal structures for different phases (Figure S3, Supporting Information), confirming the phase purity of the crystals.

Crystallography. Variable-temperature X-ray single-crystal diffraction data were collected on a Rigaku Saturn 924 diffractometer with Mo Kα radiation (λ = 0.71073 Å) at 173, 298, and 383 K. Data processing including empirical absorption corrections was performed using the CrystalClear software package (Rigaku, 2005). The structures were solved by direct methods and refined by full-matrix methods based on F^2 by means of the SHELXLTL software package. Non-H atoms were refined anisotropically using all reflections with $I > 2\sigma(I)$. All H atoms were generated geometrically and refined using a "riding" model with U_{iso} = 1.2U_{eq} (C and N). The asymmetric units and the packing views were drawn with DIAMOND (Brandenburg and Putz, 2005). Angles and distances between some atoms were calculated using DIAMOND, and other calculations were carried out using SHELXTL. Crystallographic data and structure refinement Details at 173, 298, and 383 K are given in Table 1.

Table 1. Crystal Data and Structure Refinement Details for 1 at 173, 298, and 383 K

	$2(C_6H_{14}N)_2CdCl_4$ (**1**)		
	173 K	298 K	383 K
formula wt	454.57	454.57	454.57
cryst syst	monoclinic	orthorhombic	orthorhombic
space group	*Cm*	$Cmc2_1$	*I*222
a/Å	17.874(6)	27.432(5)	28.5482(16)
b/Å	27.273(8)	8.4349(17)	6.103(4)
c/Å	11.528(5)	8.0648(16)	5.512(3)
β/deg	105.453(8)	90.00	90.00
V/Å^3, Z	5416(3), 12	1866.1(6), 4	960.4(8), 2
T_{min}/T_{max}	0.530/0.605	0.541/0.616	0.551/0.624
F(000)	2760	920	460
no. of collected/unique rflns	19896/12675	9372/2195	1743/1117
R_{int}	0.0313	0.0444	0.0767
GOF	1.087	1.083	0.926
R1 ($I > 2\sigma(I)$)	0.0452	0.0362	0.1068
wR2 ($I > 2\sigma(I)$)	0.1047	0.0592	0.2800

DSC Measurements. Differential scanning calorimetry was carried out on a PerkinElmer Diamond DSC instrument in the temperature range 170−405 K under nitrogen at atmospheric pressure in aluminum crucibles with a heating rate of 10 K/min.

Dielectric Measurements. Single-crystal samples with silver painted as the electrodes were used for dielectric studies. Complex dielectric permittivity ε ($\varepsilon = \varepsilon' - i\varepsilon''$) was measured on a Tonghui TH2828A instrument in the temperature range from 170 to 405 K and over the frequency range of 10 Hz to 1 MHz with an applied electric field of 1 V.

SHG Measurements. Polycrystalline samples were ground and sieved into particle sizes of 100−150 μm for the powder SHG measurements. An unexpanded laser beam with low divergence (pulsed Nd:YAG at a wavelength of 1064 nm, 5 ns pulse duration, 1.6 MW peak power, 10 Hz repetition rate) was used. The instrument model was FLS 920 from Edinburgh Instruments, and the temperature was 170−405 K with a cooling and heating rate of 2 K/min with the DE 202 system, while the laser was Vibrant 355 II instrument from OPOTEK. The numerical values of the nonlinear optical coefficients for SHG were determined by comparison with a KDP reference.

RESULTS AND DISCUSSION

Phase Transitions of 1. The phase transition behavior of **1** was first evidenced by the DSC measurements. Below room temperature, two reversible heat anomalies at 215 K upon heating and 212 K upon cooling were observed in the DSC curve, indicating **1** exhibits a reversible phase transition at T_1 = 215 K (Figure 1). The narrow thermal hysteresis (3 K) and the

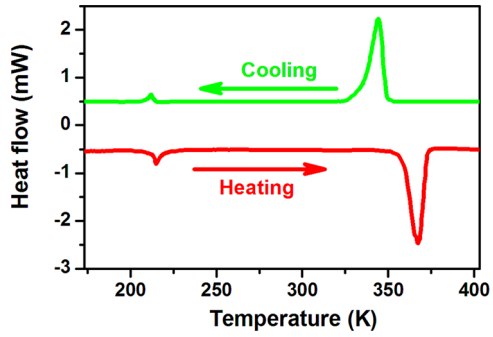

Figure 1. DSC curves of **1**.

rounded small heat anomaly peaks reveal a second-order phase transition. Above room temperature, the DSC result of **1** clearly shows that another reversible phase transition occurs at T_2 = 367 K in the heating mode with a large thermal hysteresis of 23 K (Figure 1). The combined wide thermal hysteresis and the sharp anomalous peaks support the discontinuous character of the transition, indicative of a first-order phase transition. For convenience, the phase above T_2 is designated as the high-temperature phase (HTP), the phase between T_1 and T_2 as the intermediate-temperature phase (ITP), and the phase below T_1 as the low-temperature phase (LTP).

Variable-Temperature Structures of 1. In order to investigate the details of these two structural phase transitions, we determined the crystal structures of **1** at 173, 298, and 383 K (Table 1). The three crystal structures are all non-centrosymmetric. At 173 K in the LTP, **1** crystallizes in the monoclinic crystal system, space group *Cm* (No. 8) and point group C_h. The crystal structure at 298 K in the ITP was refined in the orthorhombic space group $Cmc2_1$ (No. 36) and point group C_{2v}. Upon heating to 383 K in the HTP, the crystal structure remains orthorhombic, space group *I*222 (No. 23) and point group D_2. The cell parameters of **1** change remarkably between the LTP and ITP. In particular, the cell volume in the LTP is almost triple that in the ITP. The *a* axis length in the HTP displays a small difference from that in the ITP. However, a great change occurs in the *b* and *c* axis lengths, and the crystal volume shows an approximately 2-fold decrease.

In the LTP, the crystal structure contains infinite chains of $[CdCl_4]^-$ which are further connected to the neighboring translation-related chains by Cd···Cl weak interactions, giving rise to perovskite-type layers of corner-sharing $CdCl_6$ octahedra separated by cyclohexylammonium (CHA) cation bilayers to form an alternating inorganic−organic layered structure (Figure 2). The chains contain six independent $[CdCl_4]^-$ anions (Figure 3a). Each Cd atom, lying on the mirror symmetry plane (m) perpendicular to the *b* axis, is coordinated by two bridging and three terminal Cl atoms, forming a coordination geometry of a compressed square pyramid with basal Cd−Cl distances (2.499(2)−2.964(2) Å) longer than the apical distances (from 2.484(2) to 2.511(2) Å) (Table S1, Supporting Information). The Cd−Cl distances are consistent with those found in other structurally similar compounds.[48,49] The average Cd···Cd···Cd angle within the chain is 102.4°, giving rise to a rarely seen zigzag chain of corner-sharing $CdCl_5$ polyhedra running along

dx.doi.org/10.1021/ic501749c | Inorg. Chem. 2014, 53, 11146−11151

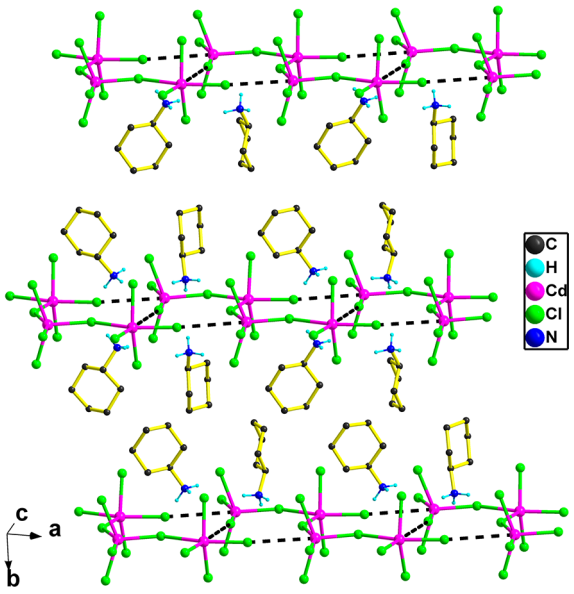

Figure 2. Alternating inorganic–organic layered structure of **1** at 173 K. The dashed lines denote the weak Cd···Cl interactions.

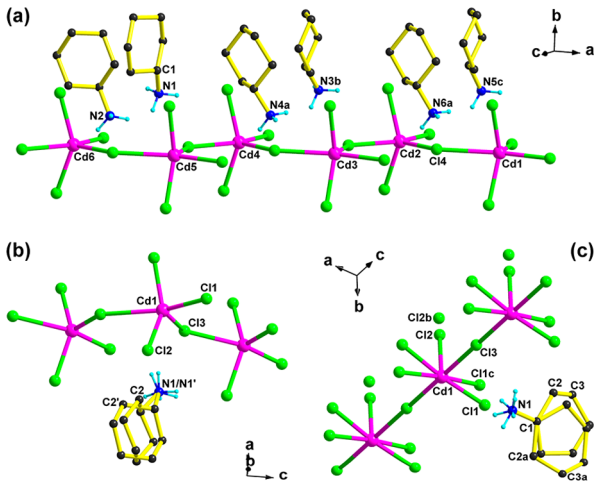

Figure 3. Asymmetric unit of **1** shown at different temperatures: (a) low-temperature phase (173 K), where the cyclohexylammonium cations are totally ordered; (b) intermediate-temperature phase (298 K), where the cyclohexylammonium cations are disordered over two sites with occupancy factors of 0.667(10) (containing C2) and 0.333(10) (containing C2′); (c) high-temperature phase (383 K), where the $[CdCl_4]_n^-$ chains become linear with the terminal Cl atoms being disordered over two positions.

the [10−1] direction (Figure 4).[48,49] The translation-related chains are connected to each other though Cd···Cl weak interactions (Cd···Cl distances, 3.903(2)−4.110(2) Å). Therefore, the coordination geometry of the Cd atoms in the crystal structure can be understood as an elongated octahedron, and correspondingly, the inorganic layers are analogous to the perovskite layers of corner-sharing $CdCl_6$ octahedra (Figure 4).[38,39] The layers are separated by CHA cations with their head NH_3 groups oriented in the cavities enclosed by the octahedrons (Figure 4). There are six independent CHA cations, all of which are ordered (Figure 3a). The ammonium groups of the CHA cations form N−H···Cl hydrogen bonds to the $[CdCl_4]_n^-$ chains with donor–acceptor distances varying

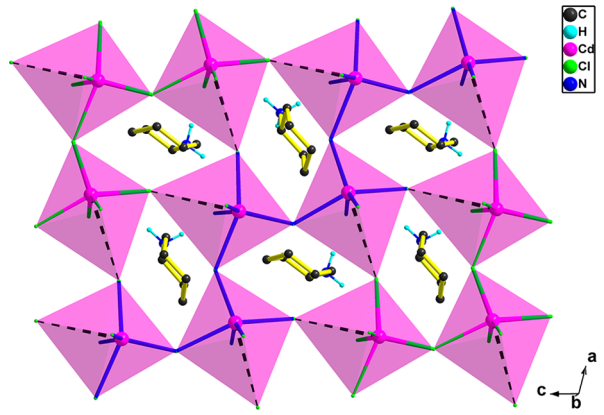

Figure 4. Packing diagram of **1** at 173 K, where the infinite zigzag $[CdCl_4]_n^-$ chain is connected to the neighboring translation-related chains though Cd···Cl weak interactions (dashed lines) to form perovskite-type layers of corner-sharing $CdCl_6$ octahedra.

from 3.147(6) to 3.468(5) Å (Figure S4 and Table S2, Supporting Information).

In the ITP, the configuration of the $[CdCl_4]_n^-$ chain extending along the *c* axis remains the same as in the LTP with a Cd···Cd···Cd angle of 101.8° (Figures 3b and 5a). The two adjacent Cd atoms are related by a 2_1-fold screw axis along the *c* axis, and accordingly the chain contains only one kind of five-coordinated Cd atom (Figures 3b and 5a). The Cd atom is still located on the *m* plane parallel to the *bc* plane and has a

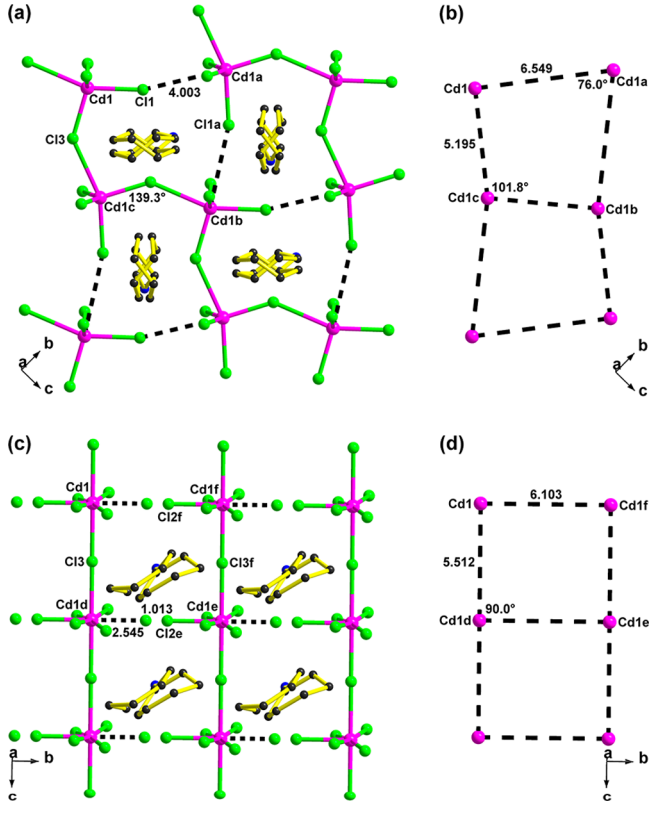

Figure 5. Packing diagrams of **1** at (a) 298 K and (c) 383 K. (b) Quadrilateral void formed by four nearest-neighbor Cd atoms at 298 K. The distances between adjacent Cd atoms are 5.195 and 6.549 Å. (d) Rectangular void formed by four nearest-neighbor Cd atoms at 383 K. The Cd···Cd distances are 5.512 and 6.103 Å.

dx.doi.org/10.1021/ic501749c | *Inorg. Chem.* 2014, 53, 11146−11151

coordination geometry similar to that in the LTP (Table S1, Supporting Information). Different from the case for the inorganic layer, the organic layer shows an obvious change in the orientation of the CHA cations. There is just one CHA cation in the asymmetric unit (Figure 3b). It is orientationally disordered over two positions with occupancy factors of 0.667(10) for the cation containing C2 and 0.333(10) for that containing C2′. The N atoms of both the major and minor components of the disordered cation act as donors for five N−H···Cl hydrogen bonds (Figure S4, Supporting Information). The average donor−acceptor distance (3.301 Å) shows no obvious change in comparison to that (3.277 Å) in the LTP (Table S2, Supporting Information). Except for the disorder of CHA cations, the inorganic−organic layered structure is similar to that in the LTP (Figure S5, Supporting Information).

The asymmetric unit in the HTP contains a CHA cation, one Cd atom, and three Cl atoms, the same as that in the ITP (Figure 3b,c). Nevertheless, the configuration of the $[CdCl_4]_n^-$ chain shows a significant change (Figure 3b,c). The terminal Cl atoms are disordered over two sites related by a 2-fold rotation axis. The Cd atom is located on the 2-fold rotation axis. The Cd−Cl bond lengths in the range 2.473(9)−2.756(6) Å change slightly (Table S1, Supporting Information), while the Cd···Cd···Cd angle within the chain becomes 180°, resulting a one-dimensional linear chain along the *c* axis (Figures 3c and 5c). The Cd···Cl distances (4.003 Å in the ITP) between adjacent chains also change, with a Cd1d···Cl2e distance of 3.558 Å (Figure 5a,c). The CHA cation in the HTP is highly disordered over two positions related by a 2-fold rotation axis along the *a* axis, which passes through the N1−C1 bond (Figure 3c). The relatively large anisotropic displacement parameters indicate the CHA cations at both positions are still disordered. The NH_3 moiety of the CHA cation is involved in seven N−H···Cl hydrogen bonds (Figure S4 and Table S2, Supporting Information). Although the $[CdCl_4]_n^-$ chains obviously change, the alternating inorganic−organic layered structure is preserved in the HTP (Figure S5, Supporting Information).

Origins of Phase Transitions of 1. It is known that disorder−order transition is one of the origins of phase transitions. From the above structural analysis, it is clear that the most notable difference between the ITP and LTP is the disorder−order transition of CHA cations. The CHA cations are orientationally disordered over two sites in the ITP, while six independent totally ordered CHA cations can be found in the LTP. It appears that the disorder−order transition of the CHA cations is responsible for the phase transition at 215 K. A precise analysis of the main packing between the ITP and HTP is needed to reveal the notable change of the $[CdCl_4]_n^-$ chain and the phase transition mechanism at 367 K. In the ITP, the void formed by four nearest-neighbor Cd atoms is a quadrilateral in the *bc* plane with two distinct pairs of Cd···Cd distances (5.195 and 6.549 Å), while in the HTP, the void becomes rectangular in the *bc* plane with Cd···Cd distance of 5.512 and 6.103 Å (Figure 5b,d). In addition, two Cd···Cd···Cd angles (101.8 and 76.0°) of the void in the ITP deviate greatly from that (90°) in the HTP (Figure 5b,d), indicating changes in the relative location of the Cd atoms in the *bc* plane after the phase transition. The elongating of Cd1···Cd1d and Cd1d···Cd1e distances in the HTP makes the Cd1−Cl3−Cd1c angle in the ITP change from 139.3 to 180° (Cd1−Cl3−Cd1d angle in the HTP) (Figure 5a,c). The Cd1d···Cl2e distance (3.558 Å) in the HTP is too long to form Cd1d−Cl2e bond, but the ionic interaction between Cd1d and Cl2e ions is still very strong, resulting in the disorder of Cl2e (Figure 5c). Furthermore, there are no Cd1a−Cl1 and Cd1b−Cl1a bonds in the ITP because of the long Cd1a···Cl1 and Cd1b···Cl1a distances (4.003 Å) (Figure 5a). After the Cd1···Cd1f and Cd1f···Cd1e distances in the HTP become shorter, a Cd1f−Cl3f bond is formed and the Cl2f atom becomes disordered (Figure 5c). Thus, the notable change in the $[CdCl_4]_n^-$ chain is induced by the changes in the relative location of the Cd atoms in the *bc* plane, which is the main driving force of the phase transition from the ITP to the HTP.

Switchable Dielectric Behaviors and Dielectric Anisotropy of 1. Crystalline materials which undergo structural phase transitions usually acquire the typical temperature-dependent dielectric states. The temperature dependence of the real part (ε') of the complex dielectric permittivity of **1** was measured on single-crystal samples along different axes with a frequency of 1000 kHz (Figure 6). The crystal faces were

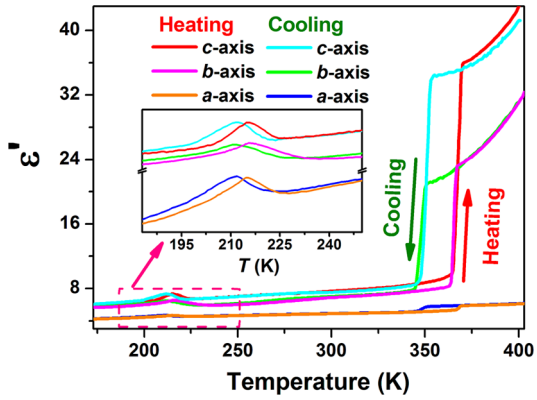

Figure 6. Real part (ε') of the complex dielectric permittivity of **1** measured along the *a*, *b*, and *c* axes at 1000 kHz.

selected in accordance with the structure in the ITP. In the heating mode, the real part along the *c* axis increases progressively until it reaches a peak value of about 7.5 at T_1, and then it exhibits a slight decrease. Thereafter, the real part shows a mild increase until the temperature gets to T_2, and suddenly it displays an abrupt change up to over 34 followed by a plateau with a gradual increase (Figure 6). The values of the real part at about 7−8 below T_2 while being over 32 above T_2 correspond to the low and high dielectric states, respectively. The transition between low and high dielectric states around T_2 makes **1** a potential high-temperature-switchable dielectric material.[6,19] In addition, clear dielectric anomalies around 344 and 212 K are also observed upon the cooling processes, in good accordance with the DSC results.

Another striking feature of the dielectric properties of **1** is the obvious anisotropy along different crystallographic axes (Figure 6). The values of ε' along the *b* and *c* axes are obviously larger than those along the *a* axis. Furthermore, notable anomalies are observed during the phase transitions, especially at 367 K along the *b* and *c* axes, while comparatively smaller anomalies are recorded in the direction of the *a* axis. The remarkable dielectric anisotropy can be explained by investigating the placement of the CHA cations and the relative location of the Cd atoms in the $[CdCl_4]_n^-$ chain. It can be seen from the structure in the ITP that the disordered CHA cation takes two positions, arousing a motion in the plane parallel to the *bc* crystallographic plane and yet perpendicular to the *a* axis (Figures 3b and 5a). Its in-plane motion only yields a very weak

dx.doi.org/10.1021/ic501749c | Inorg. Chem. 2014, 53, 11146−11151

dipole-moment component in the *a* axis, which leads to a small change of the dielectric constant in this direction. Additionally, the inorganic layer lies in the *bc* plane in the ITP. The shape of the void formed by four nearest-neighbor Cd atoms in the *bc* plane in the ITP differs much from that in the HTP (Figure 5b,d), indicating changes in the relative location of the Cd atoms along the *b* and *c* axes during the phase transition, which results in the remarkable dielectric anomalies along these two axes. The real parts of the dielectric permittivity of **1** along the *c* axis at different frequencies were also studied. The values of the real parts display slight changes at different frequencies in both the LTP (Figure S6, Supporting Information) and ITP (Figure 7). However, the real part values at lower frequencies are markedly larger than those at higher frequencies in the HTP (Figure 7).

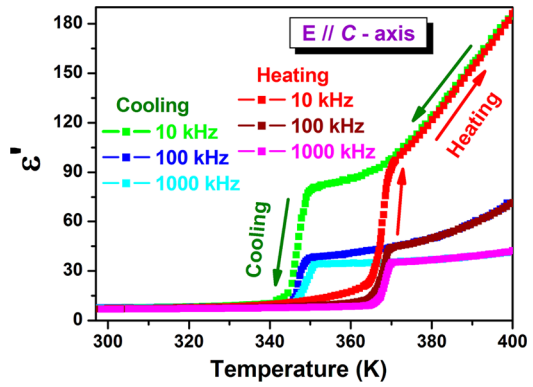

Figure 7. Real parts (ε') of the dielectric permittivity of **1** measured along the *c* axis at 10, 100, and 1000 kHz.

Switchable NLO Behaviors of 1. Generally, structural phase transitions from a noncentrosymmetric space group to a centrosymmetric space group or even another noncentrosymmetric space group will always accompany two states with different SHG responses. As depicted in Figure 8, the SHG

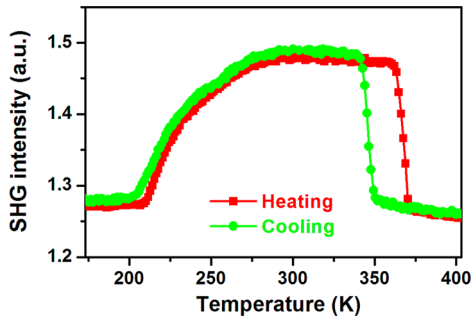

Figure 8. SHG signals of **1** as a function of temperature.

signals of **1** appear in the whole measured temperature range from 170 to 405 K, in good agreement with the space group changes from *Cm* to $Cmc2_1$ to *I*222 during the two-phase transition process. Here, it is proposed that the SHG activity of **1** mainly depends on its intrinsic structural characteristics. The Cd^{2+} ion in **1** has a closed-shell d^{10} configuration which is highly polarizable. In the $[CdCl_4]_n^-$ chain, the Cd atom is five-coordinated by two bridging and three terminal Cl atoms, making the chain lack a center of symmetry. Additionally, the adjacent anionic chains in the inorganic layers are arranged in a parallel fashion in each phase (Figure S5, Supporting Information). These structural features are conducive to crystallization of **1** in a noncentrosymmetric space group,[50−53] thus resulting in an SHG signal. The variation of SHG intensity in the vicinity of T_1 is continuous, revealing a second-order phase transition. However, at T_2, the SHG intensity decreases sharply from a high-intensity state below T_2 to a low-intensity state above T_2 (Figure 8), manifesting a first-order phase transition. The SHG intensity at room temperature is about 0.6 times that of KDP. The change trend of SHG intensity of **1** may be related to the variation of polarization, which is one of the crucial factors affecting the SHG intensity.[52−55] Since the crystal structures at both 173 K (*Cm*) and 298 K ($Cmc2_1$) assume polar space groups, the spontaneous polarization within a structural unit cell at 173 and 298 K can be approximately calculated to be 10.79 and 15.95 $\mu C/cm^2$, respectively, according to the point charge model.[56−58] The increment of spontaneous polarization may be responsible for the change in SHG intensity during the phase transition process at T_1. The shape of the void formed by four nearest-neighbor Cd atoms changing from quadrilateral in ITP to rectangular in HTP may reduce the polarization of the $[CdCl_4]_n^-$ chains, inducing the decrease of SHG intensity from ITP to HTP. Compound **1** is stable in both the high- and low-intensity states because the crystal can remain intact after a solid-to-solid structural phase transition. In addition, the two states displaying different SHG responses can be switched quickly from one to the other by stimulus of temperature, which is very consistent with the characteristics for switchable NLO.[12] Moreover, the changing trend of the SHG intensity is almost the same during the heating or cooling processes and the SHG activity could recover rapidly after 10 cycles without any attenuation, suggesting an excellent switching reversibility. Hence, these results clearly show that **1** should be treated as a potential high-temperature NLO switch.[2,12]

CONCLUSION

In summary, we have presented the one-dimensional organic−inorganic hybrid compound $[C_6H_{11}NH_3]_2CdCl_4$ with high-temperature switchable dielectric and NLO properties, which displays two structural phase transitions at 215 and 367 K. The origin of the phase transition at 215 K is attributable to the disorder−order transition of the cyclohexylammonium cations, while that of the phase transition at 367 K is associated with the changes in the relative location of Cd atoms. In addition, the dielectric and SHG switching activities at around 367 K reveal that this compound is a potential high-temperature-switchable dielectric and NLO material. We believe that this successful example will throw light on the search for new molecular compounds with multiple switchable physical properties.

ASSOCIATED CONTENT

Supporting Information

Figures, tables, and CIF files giving crystal structures, crystallographic data for the three phases, powder XRD patterns, an IR spectrum, packing views, other dielectric characterization data, selected Cd−Cl distances, and hydrogen-bond geometries. This material is available free of charge via the Internet at http://pubs.acs.org. CCDC reference numbers: 998555 (173 K), 998556 (298 K), and 998557 (383 K).

AUTHOR INFORMATION

Corresponding Author

*E-mail for Y.Z.: yizhang1980@seu.edu.cn.

Notes

The authors declare no competing financial interest.

ACKNOWLEDGMENTS

This work was supported by the Project 973 (2014CB848800), National Natural Science Foundation of China (Grants 21101025, 21201087, 21301029, and 21371032), and Jiangsu Province NSF (BK20131244, BK20130600). Also we gratefully thank Prof. Ren-Gen Xiong for revising the manuscript.

REFERENCES

(1) Feringa, B. L.; van Delden, R. A.; Koumura, N.; Geertsema, E. M. *Chem. Rev.* **2000**, *100*, 1789−1816.
(2) Champagne, B.; Plaquet, A.; Pozzo, J. L.; Rodriguez, V.; Castet, F. *J. Am. Chem. Soc.* **2012**, *134*, 8101−8103.
(3) Raymo, F. M. *Adv. Mater.* **2002**, *14*, 401−414.
(4) Irie, M.; Fukaminato, T.; Sasaki, T.; Tamai, N.; Kawai, T. *Nature* **2002**, *470*, 759−760.
(5) Kawata, S.; Kawata, Y. *Chem. Rev.* **2000**, *100*, 1777−1788.
(6) Zhang, W.; Cai, Y.; Xiong, R.-G.; Yoshikawa, H.; Awaga, K. *Angew. Chem., Int. Ed.* **2010**, *49*, 6608−6610.
(7) Sun, Z. H.; Luo, J. H.; Chen, T. L.; Li, L. N.; Xiong, R.-G.; Tong, M. L.; Hong, M. C. *Adv. Funct. Mater.* **2012**, *22*, 4855−4861.
(8) Sun, Z. H.; Wang, X. Q.; Luo, J. H.; Zhang, S. Q.; Yuan, D. Q.; Hong, M. C. *J. Mater. Chem. C* **2013**, *1*, 2561−2567.
(9) Zhou, P.; Sun, Z. H.; Zhang, S. Q.; Ji, C. M.; Zhao, S. G.; Xiong, R.-G.; Luo, J. H. *J. Mater. Chem. C* **2014**, *2*, 2341−2345.
(10) Ji, C. M.; Sun, Z. H.; Zhang, S. Q.; Chen, T. L.; Zhou, P.; Tang, Y. Y.; Zhao, S. G.; Luo, J. H. *J. Mater. Chem. C* **2014**, *2*, 6134−6139.
(11) Ji, C. M.; Sun, Z. H.; Zhang, S. Q.; Chen, T. L.; Zhou, P.; Luo, J. H. *J. Mater. Chem. C* **2014**, *2*, 567−572.
(12) Coe, B. J. *Chem. Eur. J.* **1999**, *5*, 2464−2471.
(13) Serra-Crespo, P.; van der Veen, M. A.; Gobechiya, E.; Houthoofd, K.; Filinchuk, Y.; Kirschhock, C. E. A.; Martens, J. A.; Sels, B. F.; De Vos, D. E.; Kapteijn, F.; Gascon, J. *J. Am. Chem. Soc.* **2012**, *134*, 8314−8317.
(14) Natarajan, P.; Schmittel, M. *Inorg. Chem.* **2013**, *52*, 8579−8590.
(15) Boubekeur-Lecaque, L.; Coe, B. J.; Harris, J. A.; Helliwell, M.; Asselberghs, I.; Clays, K.; Foerier, S.; Verbiest, T. *Inorg. Chem.* **2011**, *50*, 12886−12899.
(16) Wu, T.; Boyer, J. C.; Barker, M.; Wilson, D.; Branda, N. R. *Chem. Mater.* **2013**, *25*, 2495−2502.
(17) Ni, Z. P.; Ren, X. M.; Ma, J.; Xie, J. L.; Ni, C. L.; Chen, Z. D.; Meng, Q. J. *J. Am. Chem. Soc.* **2005**, *127*, 14330−14338.
(18) Thies, S.; Sell, H.; Schütt, C.; Bornholdt, C.; Nather, C.; Tuczek, F.; Herges, R. *J. Am. Chem. Soc.* **2011**, *133*, 16243−16250.
(19) Zhang, W.; Ye, H. Y.; Graf, R.; Spiess, H. W.; Yao, Y. F.; Zhu, R. Q.; Xiong, R.-G. *J. Am. Chem. Soc.* **2013**, *135*, 5230−5233.
(20) Wriedt, M.; Yakovenko, A. A.; Halder, G. J.; Prosvirin, A. V.; Dunbar, K. R.; Zhou, H. C. *J. Am. Chem. Soc.* **2013**, *135*, 4040−4050.
(21) Sun, Z. H.; Luo, J. H.; Zhang, S. Q.; Ji, C. M.; Zhou, L.; Li, S. H.; Deng, F.; Hong, M. C. *Adv. Mater.* **2013**, *25*, 4159−4163.
(22) Zhang, Y.; Liao, W. Q.; Ye, H. Y.; Fu, D. W.; Xiong, R.-G. *Cryst. Growth Des.* **2013**, *13*, 4025−4030.
(23) Bi, W.; Louvain, N.; Mercier, N.; Luc, J.; Rau, I.; Kajzar, F.; Sahraoui, B. *Adv. Mater.* **2008**, *20*, 1013−1017.
(24) Shi, X. J.; Luo, J. H.; Sun, Z. H.; Li, S. G.; Ji, C. M.; Li, L. N.; Han, L.; Zhang, S. Q.; Yuan, D. Q.; Hong, M. C. *Cryst. Growth Des.* **2013**, *13*, 2081−2086.
(25) Zhao, X. H.; Huang, X. C.; Zhang, S. L.; Shao, D.; Wei, H. Y.; Wang, X. Y. *J. Am. Chem. Soc.* **2013**, *135*, 16006−16009.
(26) Beekman, C.; Siemons, W.; Ward, T. Z.; Chi, M.; Howe, J.; Biegalski, M. D.; Balke, P.; Mksymovych, N.; Farrar, A. K.; Romero, J. B.; Gao, P.; Pan, W. Q.; Tenne, D. A.; Christen, H. M. *Adv. Mater.* **2013**, *25*, 5561−5567.
(27) Li, S. G.; Luo, J. H.; Sun, Z. H.; Zhang, S. Q.; Li, L. N.; Shi, X. J.; Hong, M. C. *Cryst. Growth Des.* **2013**, *13*, 2675−2679.
(28) Tang, Y. Y.; Ji, C. M.; Sun, Z. H.; Zhang, S. Q.; Chen, T. L.; Luo, J. H. *Chem. Asian J.* **2014**, *9*, 1771−1776.
(29) Xu, G. C.; Ma, X. M.; Zhang, L.; Wang, Z. M.; Gao, S. *J. Am. Chem. Soc.* **2010**, *132*, 9588−9590.
(30) Xu, G. C.; Zhang, W.; Ma, X. M.; Chen, Y. H.; Zhang, L.; Cai, H. L.; Wang, Z. M.; Xiong, R.-G.; Gao, S. *J. Am. Chem. Soc.* **2011**, *133*, 14948−14951.
(31) Shang, R.; Xu, G. C.; Wang, Z. M.; Gao, S. *Chem. Eur. J.* **2014**, *20*, 1146−1158.
(32) Mączka, M.; Pietraszko, A.; Macalik, B.; Hermanowicz, K. *Inorg. Chem.* **2014**, *53*, 787−794.
(33) Stoumpos, C. C.; Malliakas, C. D.; Kanatzidis, M. G. *Inorg. Chem.* **2013**, *52*, 9019−9038.
(34) Mączka, M.; Gągor, A.; Macalik, B.; Pikul, A.; Ptak, M.; Hanuza, J. *Inorg. Chem.* **2014**, *53*, 457−467.
(35) Han, J.; Nishihara, S.; Inoue, K.; Kurmoo, M. *Inorg. Chem.* **2014**, *53*, 2068−2075.
(36) Zhang, Y.; Ye, H. Y.; Zhang, W.; Xiong, R.-G. *Inorg. Chem. Front.* **2014**, *1*, 118−123.
(37) Judeinstein, P.; Sanchez, C. *J. Mater. Chem.* **1996**, *6*, 511−525.
(38) Mitzi, D. B. *Prog. Inorg. Chem.* **1999**, *48*, 1−121.
(39) Mitzi, D. B. *J. Chem. Soc., Dalton Trans.* **2001**, 1−12.
(40) Zou, C.; Zhang, Z.; Xu, X.; Gong, Q.; Li, J.; Wu, C. D. *J. Am. Chem. Soc.* **2012**, *134*, 87−90.
(41) Carlos, L. D.; Ferreira, R. A. S.; Bermudez, V. d. Z.; Julian-Lopez, B.; Escribano, P. *Chem. Soc. Rev.* **2011**, *40*, 536−549.
(42) Corma, A.; Díaz, U.; García, T.; Sastre, G.; Velty, A. *J. Am. Chem. Soc.* **2010**, *132*, 15011−15021.
(43) Kojima, N.; Okubo, M.; Shimizu, H.; Enomoto, M. *Coord. Chem. Rev.* **2007**, *251*, 2665−2673.
(44) Cai, H. L.; Zhang, Y.; Fu, D. W.; Zhang, W.; Liu, T.; Yoshikawa, H.; Awaga, K.; Xiong, R.-G. *J. Am. Chem. Soc.* **2012**, *134*, 18487−18490.
(45) Chandra, D.; Yokoi, T.; Tatsumi, T.; Bhaumik, A. *Chem. Mater.* **2007**, *19*, 5347−5354.
(46) Lin, J. G.; Su, Y.; Tian, Z. F.; Qiu, L.; Wen, L. L.; Lu, Z. D.; Li, Y. Z.; Meng, Q. J. *Cryst. Growth Des.* **2007**, *7*, 2526−2534.
(47) Mączka, M.; Ciupa, A.; Gągor, A.; Sieradzki, A.; Pikul, A.; Macalik, B.; Drozd, M. *Inorg. Chem.* **2014**, *53*, 5260−5268.
(48) Chanh, N. B.; Courseille, C.; Duplessix, R.; Meresse, A.; Couzi, M.; Tieke, B. *Mol. Cryst. Liq. Cryst.* **1990**, *188*, 261−271.
(49) Jia, H. L.; Jia, M. J.; Zeng, G.; Jin, Y.; Yu, J. H.; Xu, J. Q. *CrystEngComm* **2012**, *14*, 6599−6608.
(50) Kanis, D. R.; Ratner, M. A.; Marks, T. J. *J. Am. Chem. Soc.* **1992**, *114*, 10338−11821.
(51) Zhang, H.; Zelmon, D. E. *J. Cryst. Growth* **2002**, *234*, 529−532.
(52) Wang, C.; Zhang, T.; Lin, W. B. *Chem. Rev.* **2012**, *112*, 1084−1104.
(53) Zhang, H.; Wang, X.; Teo, B. K. *J. Am. Chem. Soc.* **1996**, *118*, 11813−11821.
(54) Di Bella, S. *Chem. Soc. Rev.* **2001**, *30*, 355−366.
(55) Zhang, W. L.; Cheng, W. D.; Zhang, H.; Geng, L.; Lin, C. S.; He, Z. Z. *J. Am. Chem. Soc.* **2010**, *132*, 1508−1509.
(56) Zhang, Y.; Ye, H. Y.; Fu, D. W.; Xiong, R.-G. *Angew. Chem., Int. Ed.* **2014**, *53*, 2114−2118.
(57) Zhang, Y.; Zhang, W.; Li, S. H.; Ye, Q.; Cai, H. L.; Deng, F.; Xiong, R.-G.; Huang, S. D. *J. Am. Chem. Soc.* **2012**, *134*, 11044−11049.
(58) Cai, H. L.; Zhang, W.; Ge, J. Z.; Zhang, Y.; Awaga, K.; Nakamura, T.; Xiong, R.-G. *Phys. Rev. Lett.* **2011**, *107*, 147601−147605.